The Astrophysical Journal Letters, 715:L30–L34, 2010 May 20 doi:10.1088/2041-8205/715/1/L30

DISCOVERY OF FOUR kpc-SCALE BINARY ACTIVE GALACTIC NUCLEI*

Xin Liu[1], Jenny E. Greene[1,3], Yue Shen[2], and Michael A. Strauss[1]
[1] Department of Astrophysical Sciences, Princeton University, Peyton Hall, Ivy Lane, Princeton, NJ 08544, USA
[2] Harvard-Smithsonian Center for Astrophysics, 60 Garden Street, MS-51, Cambridge, MA 02138, USA
Received 2010 March 9; accepted 2010 April 7; published 2010 April 30

ABSTRACT

We report the discovery of four kpc-scale binary active galactic nuclei (AGNs). These objects were originally selected from the Sloan Digital Sky Survey based on double-peaked [O III] λλ4959, 5007 emission lines in their fiber spectra. The double peaks could result from pairing active supermassive black holes (SMBHs) in a galaxy merger or could be due to bulk motions of narrow-line region gas around a single SMBH. Deep near-infrared (NIR) images and optical slit spectra obtained from the Magellan 6.5 m and the Apache Point Observatory 3.5 m telescopes strongly support the binary SMBH scenario for the four objects. In each system, the NIR images reveal tidal features and double stellar components with a projected separation of several kpc, while optical slit spectra show two Seyfert 2 nuclei spatially coincident with the stellar components, with line-of-sight velocity offsets of a few hundred km s^{-1}. These objects were drawn from a sample of only 43 objects, demonstrating the efficiency of this technique to find kpc-scale binary AGNs.

Key words: black hole physics – galaxies: active – galaxies: interactions – galaxies: nuclei – galaxies: Seyfert – quasars: general

Online-only material: color figures

1. INTRODUCTION

Despite decades of searching, and strong theoretical reasons to believe they exist, merging active supermassive black holes (SMBHs) remain difficult to find. Here we present the first four secure candidates from our ongoing search for kpc-scale binary[4] active galactic nuclei (AGNs).

It is widely appreciated that galaxies are built up hierarchically via mergers (Toomre & Toomre 1972). Since most massive galaxies are believed to harbor a central SMBH (Kormendy & Richstone 1995), galaxy mergers would result in the formation of binary SMBHs (Begelman et al. 1980; Milosavljević & Merritt 2001). Major mergers between galaxies are responsible, at least in some models, for triggering black hole accretion activity in the most luminous AGNs. Merger-based models do a decent job of fitting observational data on local SMBH demographics and AGN statistics at different cosmic epochs (e.g., Kauffmann & Haehnelt 2000; Volonteri et al. 2003; Wyithe & Loeb 2003; Hopkins et al. 2008; Shen 2009) and on the core properties of elliptical galaxies (e.g., Faber et al. 1997; Kormendy & Bender 2009), but direct observational evidence for binary SMBHs remains surprisingly scarce (e.g., Komossa et al. 2003; Bianchi et al. 2008; Rodriguez et al. 2006; Comerford et al. 2009b; Green et al. 2010).

Gerke et al. (2007) and Comerford et al. (2009a) reported two binary AGN candidates in the DEEP2 galaxy redshift survey (Davis et al. 2003), which show spatially resolved (on ∼ kpc scales) double-peaked [O III] λ5007 emission with velocity offsets of a few hundred km s^{-1}. We have selected a similar sample of 167 double-peaked [O III] narrow-line AGNs (see also Smith et al. 2009 and Wang et al. 2009 for similar statistical studies, as well as work on individual interesting objects, e.g., Xu & Komossa 2009) from the Seventh Data Release of the Sloan Digital Sky Survey (SDSS; York et al. 2000; Abazajian et al. 2009) and studied their host-galaxy and emission-line properties and selection completeness (Liu et al. 2010). The double-peaked features could be due either to narrow-line region (NLR) kinematics such as outflows or rotating disks (e.g., Axon et al. 1998; Veilleux et al. 2001; Crenshaw et al. 2010) or to a pair of AGNs. To discriminate between these scenarios for individual objects and to identify bona fide AGN pairs, we are conducting deep near-infrared (NIR) imaging and spatially resolved optical spectroscopy for the objects in the double-peaked narrow-line sample. Here, we report initial results on the discovery of four binary AGNs, SDSSJ110851.04+065901.4, SDSSJ113126.08−020459.2, SDSSJ114642.47+511029.6, and SDSSJ133226.34+060627.4. Deep NIR imaging revealed double stellar bulges in SDSSJ110851.04+065901.4, SDSSJ113126.08−020459.2, and SDSSJ133226.34+060627.4, while SDSSJ114642.47+511029.6's SDSS image shows clear evidence of a recent merger. We have obtained slit spectroscopy of all four sources. We describe our observations data analysis in Sections 2.1 and 2.2, followed by the discussion of the nature of the ionizing sources in Section 2.3. We discuss our results and conclude in Section 3. A cosmology with $\Omega_m = 0.3$, $\Omega_\Lambda = 0.7$, and $h = 0.7$ is assumed throughout.

2. OBSERVATIONS AND DATA ANALYSIS

2.1. NIR Imaging

We obtained K_s and J images for SDSSJ113126.08−020459.2, a K_s image for SDSSJ110851.04+065901.4, and a J image for SDSSJ133226.34+060627.4 on the nights of 2009 December 29 through 2010 January 2 UT using the Persson's Auxiliary Nasmyth Infrared Camera (PANIC; Martini et al. 2004) on the 6.5 m Magellan I (Baade) telescope. PANIC has a $2' \times 2'$ field of view (FOV) and $0''.126$ pixels. The observing conditions were clear but not photometric, with seeing

* This Letter includes data gathered with the 6.5 m Magellan telescopes located at Las Campanas Observatory, Chile, and with the Apache Point Observatory 3.5 m telescope, which is owned and operated by the Astrophysical Research Consortium.
[3] Princeton-Carnegie Fellow.
[4] We refer to both a bound pair of SMBHs in a Keplerian orbit and a pair of SMBHs at large separations where the galactic potential dominates, as *binaries*.

Table 1
Host-galaxy and Emission-line Properties

SDSS Designation	Redshift	M_*	K_s	$g-r$	$J-K_s$	$\Delta\theta_i$ ($''$)	ΔS_i (kpc)	L_1/L_2	$L_{[\mathrm{O\,III}]_1}$	$L_{[\mathrm{O\,III}]_2}$	$\Delta\theta_{[\mathrm{O\,III}]}$ ($''$)	$\Delta\theta_{\mathrm{H}\alpha}$ ($''$)	n_{e_1}	n_{e_2}
(1)	(2)	(3)	(4)	(5)	(6)	(7)	(8)	(9)	(10)	(11)	(12)	(13)	(14)	(15)
SDSSJ110851.04+065901.4	0.1816	11.0	14.29	0.8	1.3	0.5	1.5	1.0	8.58	7.94	0.9	0.6	$2.4^{+0.1}_{-0.2}$	$2.4^{+0.7}_{-1.3}$
SDSSJ113126.08−020459.2	0.1463	11.3	14.51	1.0	1.3	0.6	1.5	1.8	7.81	7.72	0.6	0.6	$2.7^{+0.2}_{-0.4}$	$-0.3^{+1.7}_{-0.7}$
SDSSJ114642.47+511029.6	0.1300	10.9	14.32	1.0	1.4	2.7	6.3	0.9	8.35	7.79	2.5	2.8	$3.1^{+0.5}_{-0.4}$	$2.9^{+1.0}_{-0.4}$
SDSSJ133226.34+060627.4	0.2070	11.1	14.72	1.2	1.6	1.5	5.1	1.6	7.48	8.25	1.6	1.6	$2.8^{+0.4}_{-0.8}$	$2.4^{+0.3}_{-0.5}$

Notes. The subscripts "1" and "2" denote blueshifted and redshifted components. Column 3: total stellar masses in the form of $\log(M_*/M_\odot)$ for the whole galaxy based on SDSS photometry from Kauffmann et al. (2003); Column 4: from 2MASS; Column 5: color from SDSS photometry; Column 6: color from 2MASS; Columns 7 and 8: projected separation based on NIR imaging; Column 9: J- (for SDSSJ133226.34+060627.4) or Ks-band (for the others) luminosity ratio of the two stellar bulges estimated with aperture photometry; Columns 10 and 11: blueshifted and redshifted [O III] λ5007 component luminosities in the form of $\log(L/L_\odot)$; Column 12: projected spatial offset measured from [O III] λ5007; Column 13: projected spatial offset measured from Hα and [N II]; Columns 14 and 15: electron density in the form of $\log(n_e/\mathrm{cm}^{-3})$ of the blueshifted and redshifted components.

ranging between 0.″5 and 0.″8 in the optical. Total exposure times were 1080 s and 2160 s in K_s for SDSSJ110851.04+065901.4 and SDSSJ113126.08−020459.2, respectively, and 1080 s in J for both SDSSJ113126.08−020459.2 and SDSSJ133226.34+060627.4. We reduced PANIC data with the Carnegie Supernova Project pipeline (Hamuy et al. 2006) following standard procedures.

Figure 1 shows the K_s image for SDSSJ114642.47+511029.6 from Two Micron All Sky Survey (2MASS; Skrutskie et al. 2006) and the K_s images for SDSSJ110851.04+065901.4 and SDSSJ113126.08−020459.2 and the J image for SDSSJ133226.34+060627.4. Also presented are the SDSS r-band images to illustrate the galaxy-scale environment and tidal features. The NIR images show two stellar bulges in each of these systems. In addition, all four systems show tidal features suggestive of mergers. For SDSSJ114642.47+511029.6, this is clearly seen in its SDSS image; in SDSSJ110851.04+065901.4, SDSSJ113126.08−020459.2, and SDSSJ133226.34+060627.4, the SDSS images show tentative tidal features which are confirmed in deep PANIC images. The PANIC image of SDSSJ110851.04+065901.4 also reveals a small companion (∼3″ west to the nuclei) which is barely resolved in its SDSS image. The two stellar nuclei in SDSSJ110851.04+065901.4 appear marginally resolved in the center; their SDSS counterparts exhibit different colors which could indicate different stellar populations or dust effects. We performed aperture photometry for the two stellar nuclei to infer their luminosity ratio. Table 1 lists the estimated luminosity ratios in K_s or in J. Assuming similar mass-to-light ratios in the two stellar nuclei, they all appear to be major mergers with comparable stellar masses. Also listed in Table 1 are the projected separation $\Delta\theta_i$, the stellar mass of the whole galaxy estimated based on SDSS photometry (Kauffmann et al. 2003), and the 2MASS K_s magnitudes and $K_s - J$ colors.

2.2. Optical Slit Spectroscopy

Because of the lack of spatial information in the SDSS spectra, it is unclear whether the two velocity components seen in [O III] are spatially associated with the two stellar bulges. To resolve this question, we obtained slit spectra for SDSSJ110851.04+065901.4, SDSSJ113126.08−020459.2, and SDSSJ133226.34+060627.4 on the nights of 2010 January 12 through 14 UT using the Low-Dispersion Survey Spectrograph (LDSS3) on the 6.5 m Magellan II (Clay) telescope. The observing conditions were clear but not photometric, with seeing ranging between 0.″7 and 1.″1. LDSS3

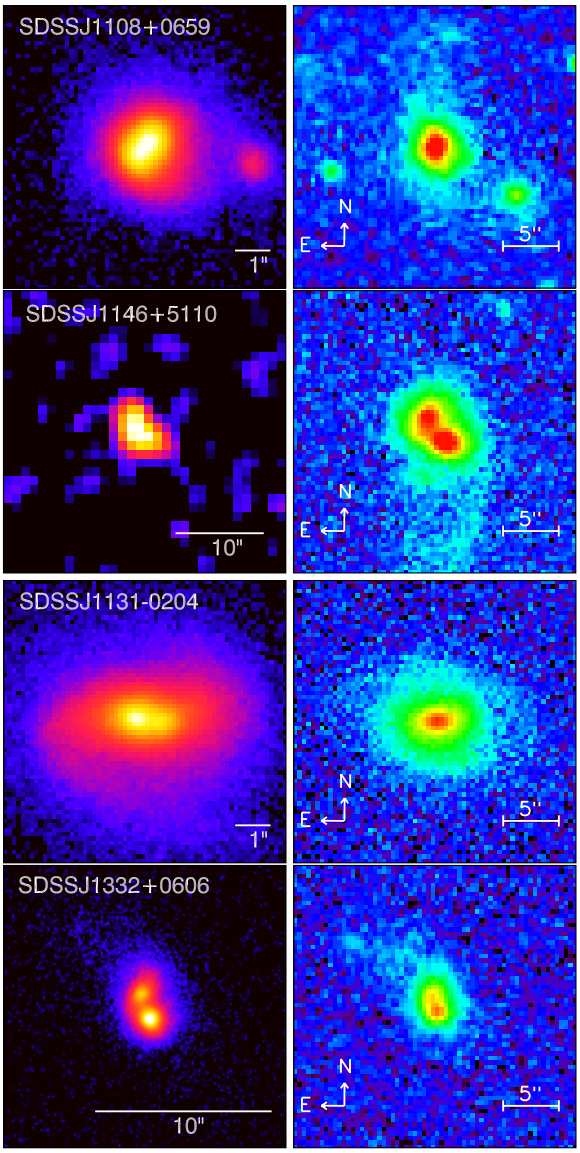

Figure 1. Left: NIR images for SDSSJ114642.47+511029.6 (K_s) from 2MASS and for SDSSJ110851.04+065901.4 (K_s), SDSSJ113126.08−020459.2 (K_s), and SDSSJ133226.34+060627.4 (J) from our PANIC observations. North is up and east is to the left. Spatial scales are indicated on each panel. Colors are an asinh scale to intensity with a stretch to highlight the central nuclei. Right: SDSS r-band images to show tidal features and galaxy-scale environment.

(A color version of this figure is available in the online journal.)

has a 8.′3 diameter FOV and 0.″188 pixels. We employed a $1'' \times 4'$ long slit with the Volume Phase Holographic (VPH)-blue grism to cover Hβ and [O III] $\lambda\lambda$4959, 5007, and the VPH-red grism (with the OG590 filter) to cover Hα and [N II]. We oriented the slit to go through the two stellar bulges seen in the NIR images (with P.A. = 141°, 80°, and 17° for SDSSJ110851.04+065901.4, SDSSJ113126.08−020459.2, and SDSSJ133226.34+060627.4, respectively). The spectral resolution was 3.1 (6.3) Å FWHM in the blue (red). Total exposure times were 4800 s, 6300 s, and 4500 s for SDSSJ110851.04+065901.4, SDSSJ113126.08−020459.2, and SDSSJ133226.34+060627.4, respectively, in the blue, and 1800 s for all three objects in the red. We took wavelength calibration spectra and flat fields after observing each object. We obtained spectra for SDSSJ114642.47+511029.6 on the night of 2010 February 15 UT using the Dual Imaging Spectrograph (DIS) on the Apache Point Observatory 3.5 m telescope. The sky was photometric, albeit with poor seeing ranging between 1.″7 and 2.″7. DIS has a $4' \times 6'$ FOV and 0.″414 pixels. We adopted a $1.''5 \times 6'$ slit and the B1200+R1200 gratings centered at 5500 and 7450 Å. The slit was oriented with P.A. = 59° to go through both bulges shown in the SDSS image. The spectral resolution was 1.8 (1.3) Å FWHM in the blue (red). The total exposure time was 4800 s. We reduced the DIS and LDSS3 data following standard IRAF[5] procedures (Tody 1986) and with the COSMOS reduction pipeline.[6] We observed white dwarfs EG21 and G191B2B for spectrophotometric calibration. We applied a telluric correction from our standard stars after extracting one-dimensional (1D) spectra.

The spatial correspondence between the two stellar continuum peaks and two [O III] velocity peaks in all cases strongly indicates we are seeing two active galaxies (Figure 2). We see unambiguous spatial separations between the red and blue velocity components in all targets and in each strong emission line. We measure this spatial offset, $\Delta\theta_e$, from a spatial profile summed over twice the FWHM of each line (although we combine Hα and [N II] due to blending). We also checked these results by directly examining the two-dimensional (2D) flux-density profile of each velocity component. The spatial offsets derived from each strong line (Hβ, [O III] λ4959, [O III] λ5007 ($\Delta\theta_{[\mathrm{O\,III}]}$ in Table 1), and the Hα-[N II] region ($\Delta\theta_{\mathrm{H}\alpha}$ in Table 1)) agree within ∼0.″3. Note in the case of SDSSJ114642.47+511029.6, the [O III] $\lambda\lambda$4959, 5007 lines fall in the dichroic edge and are poorly detected in the redshifted component,[7] but the spatial separation is clearly measured in the Hα and [N II] lines. The separation between the two velocity components of the emission lines is consistent with that of the double stellar bulges ($\Delta\theta_i$ in Table 1). More directly, the emission lines are coincident with the stellar continua seen in the spectra. This spatial coincidence suggests that the double-peaked emission-line profiles in the SDSS spectra of these objects are due to the orbital motion of the gas associated with the double stellar bulges. This is further supported by the tidal features indicative of mergers seen in all four systems (Section 2.1, Figure 1).

2.3. The Nature of the Ionizing Sources

The nature of the ionizing source in each object is constrained using the Baldwin–Phillips–Terlevich diagram (Baldwin et al. 1981; Veilleux & Osterbrock 1987) featuring the emission-line ratios [O III] λ5007/Hβ and [N II] λ6584/Hα (Figure 3). We fit multi-component models to the emission lines over the stellar-continuum-subtracted LDSS3 and DIS spectra (refer to Liu et al. 2010 for details on constructing continuum models and emission-line fitting) and measured line ratios. For SDSSJ110851.04+065901.4, SDSSJ113126.08−020459.2, and SDSSJ133226.34+060627.4, we extracted 1D spectra summing over both velocity components as they are partially blended spatially, whereas for SDSSJ114642.47+511029.6 we extracted 1D spectra separately for each of the two velocity components. We compared measurements based on the SDSS and the LDSS3 and DIS spectra and found general agreement in the line ratios; the difference in line fluxes is likely due to the difference in the fiber and slit coverage. Figure 2 (bottom panels) shows an example of our emission-line fits and of the difference in SDSS and slit spectra. In all cases, the diagnostic line ratios indicate Seyfert-type ionization (except for the redshifted component in SDSSJ114642.47+511029.6, which could also be a LINER or a composite). Table 1 lists [O III] λ5007 luminosities for both velocity components based on our LDSS3/DIS spectra.

While the diagnostic line ratios indicate the presence of hard ionizing photons, it is ambiguous whether there are two ionizing sources. If only one nucleus were to ionize both gas components, the ionization parameter in the off-nuclear region would be much lower than that in the nuclear region with similar electron densities, because the number density of ionizing photons decays as r^{-2}. We measured electron densities n_e using the diagnostic line ratio [S II] λ6717/[S II] λ6731. For SDSSJ110851.04+065901.4, SDSSJ114642.47+511029.6, and SDSSJ133226.34+060627.4, we found comparable n_e values in the two velocity components (Table 1). The comparable electron densities and high ionization states (Figure 3) in both narrow-line components suggest that there are separate hard ionizing sources associated with each line component. For SDSSJ113126.08−020459.2, the inferred n_e of the redshifted component is ∼1000 times smaller than the blueshifted component, but the uncertainties of the measurement are so large that they may differ by no more than a factor of ∼10. Considering typical n_e values of NLR gas in stellar bulges, in SDSSJ113126.08−020459.2 the comparable and high [O III] λ5007/Hβ ratios may still argue for separate ionizing sources, but it is possible that the nucleus associated with the blueshifted component is ionizing both velocity components. *Chandra* observations would clarify the situation considerably. To summarize, our imaging and spectroscopy data strongly support the binary AGN scenario for at least three of the four objects.

3. DISCUSSION

As listed in Table 1, the four new kpc-scale binary AGNs that we have presented here have optical colors typical of type 2 AGNs (e.g., Kauffmann et al. 2003). All four objects show tidal features suggestive of mergers (Section 2.1, Figure 1). Among them, SDSSJ110851.04+065901.4 was detected (but unresolved) in FIRST with an integrated flux of

[5] IRAF is distributed by the National Optical Astronomy Observatories, which are operated by the Association of Universities for Research in Astronomy (AURA) under cooperative agreement with the National Science Foundation.

[6] http://www.ociw.edu/Code/cosmos

[7] In SDSSJ114642.47+511029.6, the blueshifted component itself shows double peaks which also appear spatially offset from one another; our measurements for the blueshifted component represent the luminosity-weighted average of both peaks. The redshifted component overlaps with the redshifted peak of the blueshifted component in velocity space, and we extracted 1D spectra for the two components separately to disentangle them properly.

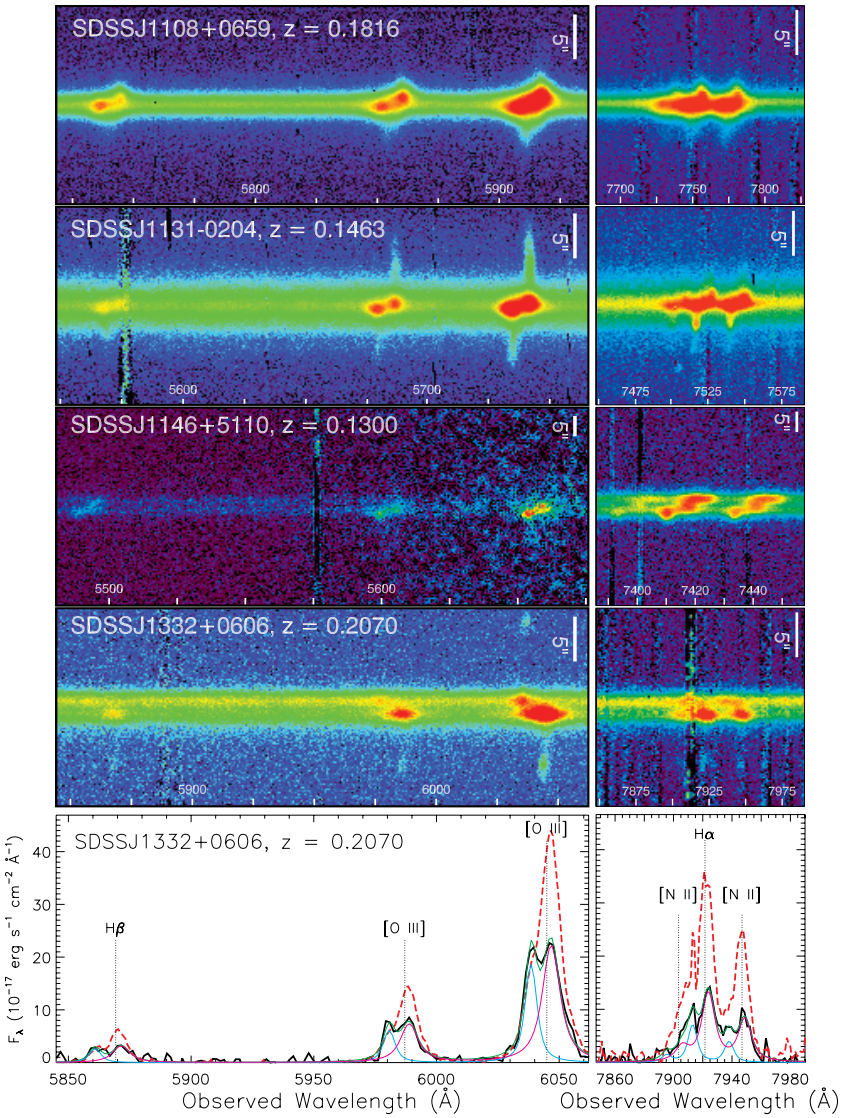

Figure 2. Top four rows: LDSS3 and DIS 2D spectra over the Hβ-[O III] (left column) and Hα-[N II] (right column) regions. Colors indicate flux densities with asinh scales and a stretch to illustrate both nuclei and extended emission. In both SDSSJ114642.47+511029.6 and SDSSJ133226.34+060627.4, the blueshifted (redshifted) component corresponds to the SW (NE) stellar bulge in its image (Figure 1). In SDSSJ113126.08−020459.2, the blueshifted (redshifted) component corresponds to the E (W) bulge in its image, while in SDSSJ110851.04+065901.4, the blueshifted (redshifted) component corresponds to the NW (SE) bulge in its image. Bottom row: stellar-continuum-subtracted spectra for SDSSJ133226.34+060627.4 from LDSS3 (red, dashed curves) and from SDSS (data in black, best-fit model in green, and the two velocity components in cyan and magenta). The vertical dotted lines are drawn at the systemic redshift of each object as measured from stellar absorption features. In SDSSJ133226.34+060627.4, the SDSS fiber covered only part of the redshifted component.

(A color version of this figure is available in the online journal.)

9.84±0.13 mJy (White et al. 1997); it also has a candidate match in the *IRAS* Faint Source Catalog (Moshir et al. 1992), IRAS F11062+0715, with $L_{\rm IR} \sim 10^{12}\,L_\odot$, although the positional match is only marginal (∼9.″5 offset from its SDSS position). SDSSJ113126.08−020459.2, SDSSJ114642.47+511029.6, and SDSSJ133226.34+060627.4 were not detected in FIRST or in *IRAS*. At least three of the four galaxies appear to be neither star-bursting luminous IR galaxies (LIRGs) nor passively evolving ellipticals. These properties are in contrast to the few existing samples of known kpc-scale binary AGNs, which tend to be found either in LIRGs which involve gas-rich mergers of disks (NGC 6240: Komossa et al. 2003; Mrk 463: Bianchi et al. 2008; Arp 299: Ballo et al. 2004) or in ellipticals at the centers of galaxy clusters and power twin jets (3C 75: Owen et al. 1985; PKS 2149−158: Guidetti et al. 2008). Perhaps this reflects our differing selecting criteria, but we are hopeful that with our systematic approach we can begin to characterize the evolutionary state of kpc-scale binary AGNs in more detail. Further host-galaxy studies on these four binary AGNs including their structural properties, stellar populations, and dynamics, as well as the remainder of our NIR imaging subsample will be presented elsewhere.

Until recently, searches for kpc-scale binary AGNs have been more or less serendipitous. We have demonstrated with the observations presented in this Letter that selecting spectroscopic candidates based on double-peaked narrow lines and follow-up with high spatial resolution imaging and spectroscopy is a promising technique to identify genuine binary AGNs in an efficient and systematic way. Out of the 43 objects observed so far, we detected three, and perhaps four binary AGNs (∼7%–10%). These four systems probe the relatively early stages of AGN pairing, when the two stellar bulges which

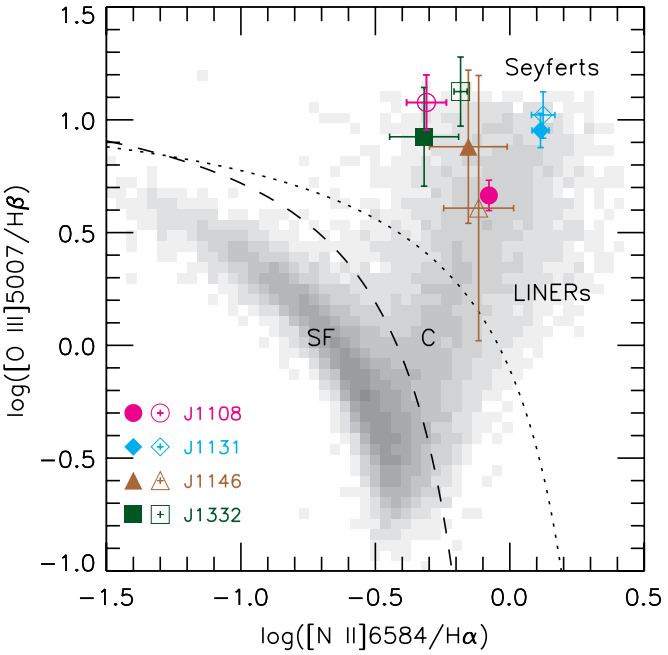

Figure 3. Diagnostic line ratios measured from our LDSS3 and DIS spectra. In each system, the two velocity components are plotted using the same color, with the filled (open) symbol denoting the blueshifted (redshifted) component. Gray scales indicate number densities of 31,179 emission-line galaxies from the SDSS DR4 (Kauffmann et al. 2003). Also shown is the theoretical starburst limit (dotted curve) from Kewley et al. (2001) along with the empirical separation (dashed curve) between H II regions and AGNs (Kauffmann et al. 2003). Pure star-forming (SF) galaxies lie below the dashed curve, AGN-dominated objects lie above the dotted curve, and H II–AGN composites (C) lie in between.

(A color version of this figure is available in the online journal.)

host the two SMBHs are still separated enough to show two distinct components in IR/optical images. The ∼10% lower limit translates into a 0.1% kpc-scale binary AGN fraction out of the parent AGN sample (167 double-peaked objects selected from 14,756 AGNs; Liu et al. 2010), comparable to the binary quasar fraction with projected separations of tens of kpc (Hennawi et al. 2006, 2009; Myers et al. 2008), albeit with different systematics and potential selection biases. We also have objects in our sample in which the [O III] emission is spatially resolved but the NIR continuum is not, and in a few such cases the spatially resolved spectrum shows clear signs of a velocity gradient across the slit, suggesting a rotation/outflow origin for the double-peaked profile. Thus, it is premature to claim a binary AGN based on spatially resolved [O III] emission alone. A detailed analysis on the fraction of such "false positives" and their properties will be presented in a future paper.

We are conducting NIR imaging of the rest of our double-peaked narrow-line sample using Magellan and Keck with adaptive optics. Together with follow-up spectroscopy, we expect to increase the number of known kpc-scale binary AGNs several folds. High-quality multi-band data will allow us to explore the properties of individual binary AGNs in great detail, and the increased statistics will provide important constraints on the merger hypothesis, AGN lifetimes, and the interplay between SMBHs and their hosts.

We thank J. Krolik for interesting comments, and the anonymous referee for a prompt report. X.L. and M.A.S. acknowledge the support of NSF grant AST-0707266. Y.S. acknowledges support from a Clay Postdoctoral Fellowship through the Smithsonian Astrophysical Observatory.

Funding for the SDSS and SDSS-II has been provided by the Alfred P. Sloan Foundation, the Participating Institutions, the National Science Foundation, the U.S. Department of Energy, the National Aeronautics and Space Administration, the Japanese Monbukagakusho, the Max Planck Society, and the Higher Education Funding Council for England. The SDSS Web site is http://www.sdss.org/.

Facilities: Sloan, Magellan:Baade (PANIC), ARC(DIS)

REFERENCES

Abazajian, K. N., et al. 2009, ApJS, 182, 543
Axon, D. J., Marconi, A., Capetti, A., Maccetto, F. D., Schreier, E., & Robinson, A. 1998, ApJ, 496, L75
Baldwin, J. A., Phillips, M. M., & Terlevich, R. 1981, PASP, 93, 5
Ballo, L., Braito, V., Della Ceca, R., Maraschi, L., Tavecchio, F., & Dadina, M. 2004, ApJ, 600, 634
Begelman, M. C., Blandford, R. D., & Rees, M. J. 1980, Nature, 287, 307
Bianchi, S., Chiaberge, M., Piconcelli, E., Guainazzi, M., & Matt, G. 2008, MNRAS, 386, 105
Comerford, J. M., et al. 2009a, ApJ, 698, 956
Comerford, J. M., Griffith, R. L., Gerke, B. F., Cooper, M. C., Newman, J. A., Davis, M., & Stern, D. 2009b, ApJ, 702, L82
Crenshaw, D. M., Schmitt, H. R., Kraemer, S. B., Mushotzky, R. F., & Dunn, J. P. 2010, ApJ, 708, 419
Davis, M., et al. 2003, Proc. SPIE, 4834, 161
Faber, S. M., et al. 1997, AJ, 114, 1771
Gerke, B. F., et al. 2007, ApJ, 660, L23
Green, P. J., Myers, A. D., Barkhouse, W. A., Mulchoey, J. S., Bennert, V. N., Cox, T. J., & Aldcroft, T. L. 2010, ApJ, 710, 1578
Guidetti, D., Murgia, M., Govoni, F., Parma, P., Gregorini, L., de Ruiter, H. R., Cameron, R. A., & Fanti, R. 2008, A&A, 483, 699
Hamuy, M., et al. 2006, PASP, 118, 2
Hennawi, J. F., et al. 2006, AJ, 131, 1
Hennawi, J. F., et al. 2009, arXiv:0908.3907
Hopkins, P. F., Hernquist, L., Cox, T. J., & Kereš, D. 2008, ApJS, 175, 356
Kauffmann, G., & Haehnelt, M. 2000, MNRAS, 311, 576
Kauffmann, G., et al. 2003, MNRAS, 346, 1055
Kewley, L. J., Dopita, M. A., Sutherland, R. S., Heisler, C. A., & Trevena, J. 2001, ApJ, 556, 121
Komossa, S., Burwitz, V., Hasinger, G., Predehl, P., Kaastra, J. S., & Ikebe, Y. 2003, ApJ, 582, L15
Kormendy, J., & Bender, R. 2009, ApJ, 691, L142
Kormendy, J., & Richstone, D. 1995, ARA&A, 33, 581
Liu, X., Shen, Y., Strauss, M. A., & Greene, J. E. 2010, ApJ, 708, 427
Martini, P., Persson, S. E., Murphy, D. C., Birk, C., Shectman, S. A., Gunnels, S. M., & Koch, E. 2004, Proc. SPIE, 5492, 1653
Milosavljević, M., & Merritt, D. 2001, ApJ, 563, 34
Moshir, M., Kopman, G., & Conrow, T. A. O. (ed.) 1992, IRAS Faint Source Survey, Explanatory Supplement, version 2 (Pasadena, CA: Infrared Processing and Analysis Center, California Institute of Technology)
Myers, A. D., Richards, G. T., Brunner, R. J., Schneider, D. P., Strand, N. E., Hall, P. B., Blomquist, J. A., & York, D. G. 2008, ApJ, 678, 635
Owen, F. N., O'Dea, C. P., Inoue, M., & Eilek, J. A. 1985, ApJ, 294, L85
Rodriguez, C., Taylor, G. B., Zavala, R. T., Peck, A. B., Pollack, L. K., & Romani, R. W. 2006, ApJ, 646, 49
Shen, Y. 2009, ApJ, 704, 89
Skrutskie, M. F., et al. 2006, AJ, 131, 1163
Smith, K. L., Shields, G. A., Bonning, E. W., McMullen, C. C., & Salviander, S. 2009, arXiv:0908.1998
Tody, D. 1986, Proc. SPIE, 627, 733
Toomre, A., & Toomre, J. 1972, ApJ, 178, 623
Veilleux, S., & Osterbrock, D. E. 1987, ApJS, 63, 295
Veilleux, S., Shopbell, P. L., & Miller, S. T. 2001, AJ, 121, 198
Volonteri, M., Haardt, F., & Madau, P. 2003, ApJ, 582, 559
Wang, J., Chen, Y., Hu, C., Mao, W., Zhang, S., & Bian, W. 2009, ApJ, 705, L76
White, R. L., Becker, R. H., Helfand, D. J., & Gregg, M. D. 1997, ApJ, 475, 479
Wyithe, J. S. B., & Loeb, A. 2003, ApJ, 595, 614
Xu, D., & Komossa, S. 2009, ApJ, 705, L20
York, D. G., et al. 2000, AJ, 120, 1579